# Capture of $H_2S$ from Binary Gas Mixture by Imidazolium-Based Ionic Liquids with Nonfluorous Anions: A Theoretical Study

**Jie-Jie Chen, Wen-Wei Li, and Han-Qing Yu**
Dept. of Chemistry, University of Science & Technology of China, Hefei 230026, China

**Xue-Liang Li**
Anhui Key Laboratory of Controllable Chemistry Reaction & Material Chemical Engineering, School of Chemical Engineering, Hefei University of Technology, Hefei 230009, China

*DOI 10.1002/aic.14111*
*Published online April 19, 2013 in Wiley Online Library (wileyonlinelibrary.com)*

*Selective capture of $H_2S$ from gas mixture is essential to reduce its undesirable high corrosiveness and toxicity. Ionic liquids have been proposed as a promising material, and there is a need to clarify the capture mechanisms and search for optimal combination of cation and anion for application. This work aims to elucidate the interactions between $H_2S$ and nonfluorous imidazolium ionic liquids (NIILs) at a molecular level. The effects of hydroxyl group on the tail of alkyl chain, and combinations of imidazolium cations and nonfluorous anions on $H_2S$ capture are explored using quantum chemistry calculations. Furthermore, molecular dynamics simulations are used to explore the microstructural features of NIIL–$H_2S$–$CH_4$ mixture systems. It is found that the hydroxyl groups in the cations is essential in governing the absorption properties of NIILs, including the interaction sites for hydrogen bonding, interaction geometries and energies, diffusion coefficients, and organization of $H_2S$ and $CH_4$ around cations and anions. A molecular viewpoint to design appropriate ionic liquids for promoting their applications for $H_2S$ capture is provided.* © 2013 American Institute of Chemical Engineers *AIChE J*, 59: 3824–3833, 2013

*Keywords: nonfluorous imidazolium ionic liquids (NIILs), $H_2S$, quantum chemistry calculation, molecular dynamics simulation, topological characteristics, interaction energy, radial distribution function, diffusion coefficient*

## Introduction

Hydrogen sulfide ($H_2S$) is widely present in natural gas fields, various industrial waste-gas streams and biogas generated from anaerobic fermentation of wastes. Typical processes involving $H_2S$ release include hydrodesulphurization of crude oils and reduction of heavy metal ions in ground and surface waters by sulfate metal reducing bacteria.[1,2] Because of its undesirable high corrosiveness and toxicity, $H_2S$ should be removed from industrial gases, oil streams, and biogas,[3] and several methods[4–7] have been proposed for such purposes. One common method for natural gas sweetening is chemical absorption using amine aqueous solutions, mainly consisting of alkanolamines.[1,7,8] Although the amine processes have been used for decades, there are some technical problems to be resolved, such as transfer of water into gas stream, degradation of alkanolamine to form corrosive byproducts and secondary pollution due to its high volatility.[9] In comparison, the ionic liquids (ILs) are considered to be more appropriate materials for $H_2S$ capture, attributed to their negligible vapor pressures, high thermal and chemical stability, tunable properties, and excellent $H_2S$ solubility.[2,10–14] Thus, ILs absorption offers an efficient, cost-effective, and environmental-beneficial way for gas sweetening solutions. The absorption capacity of ILs is affected by temperature, pressure, and structure of cations and anions.[11,12] For example, when 1-*n*-butyl-3-methyl-imidazolium [bmim] is used as the cation, the $H_2S$ solubility in ILs with bis[trifluoromethylsulfonyl]amide anion ($Tf_2N^-$) is higher than those with hexafluorophosphate ($PF_6^-$) and tetrafluoroborate ($BF_4^-$).[11] However, when the cation is changed to 1-*n*-hexyl-3-methylimidazolium [hmim], the $BF_4^-$-containing ILs show a higher $H_2S$ solubility than the other ILs.[12] This suggests that different combinations of cation and anion can lead to significantly different characteristics of ILs.[15,16] Thus, the optimal combinations should be pursued for applications.

The type of anion also influences the solubility of acid gas in ILs. For example, anion has been found to significantly affect the $CO_2$ solubility.[17,18] Fluorine atom containing anions (fluorous anions) have been reported as efficient anions of ILs for $H_2S$ absorption.[13] However, such ILs are expensive[19] and a potential environmental pollutant.[20] In this respect, ILs with nonfluorous anions,[21] such as lactate anion (LAC),[9] alkylsulfate anions,[22,23] and amino acid ions,[24,25] appear to be more attractive alternatives. Among them, methylsulfate anion ($MeSO_4$) has been found to efficiently separate $H_2S$ from $CO_2$,[22] whereas the LAC is generally regarded as safe anion groups. The interaction mechanism between $H_2S$ and these two nonfluorous anions may provide valuable information for applications.

Additional Supporting Information may be found in the online version of this article.

Correspondence concerning this article should be addressed to X.-L. Li at lixuel987@163.com (or) H.-Q. Yu at hqyu@ustc.edu.cn.

In addition to anions, the cations of ILs also pose significant impacts on acid gas absorption.[26] ILs with imidazolium cations have been widely used for $H_2S$ removal, attributed to their high thermal and chemical stability. Furthermore, the conventional amine aqueous solution, for example, monoethanolamine, diethanolamine, and methyldiethanolamine, have hydroxyl group on the tail of the alkyl chain. Thus, the widely used cation, [bmim], was chosen and the hydroxyl group was attached on each side chain separately. With a combination of two anions of LAC and $MeSO_4$, six possible nonfluorous imidazolium ionic liquids (NIILs) are available for comparing their $H_2S$ capturing capacities.

The main objective of this work is to design and develop efficient NIILs with different cation and anion combinations for selectively capturing $H_2S$ from $H_2S$—$CH_4$ mixture and elucidate the interaction mechanisms. Theoretical data[27,28] on the nature of the interactions between $H_2S$ and NIIL components may be useful to determine and prepare the most appropriate NIIL for $H_2S$ capture. The interactions between $H_2S$ and the NIILs are explored via quantum chemistry (QC) calculations based on density functional theory with dispersion correction (DFT-D) to give an insight into the effective absorption sites at the molecular level. Structural features and the diffusivities of gases in NIILs, which is the key information needed in IL design, are evaluated using molecular dynamics (MD) simulations for the mixture of NIILs and gases with $H_2S$ and $CH_4$.

## Computational Methods

### *DFT-D calculations*

DFT-D computation is used to identify the structures of NIILs and their absorption products. For the interaction calculation, an all-electron method, which is within the Perdew–Wang 91 (PW91) and Perdew, Burke, and Ernzerhof (PBE) forms of generalized gradient approximation[29] for the exchange-correlation term, is used as implemented in the DMol$^3$ code.[30] In the geometry optimization, the positions of all the atoms are fully relaxed, in order to locate the global minimum on the potential energy surface; other local minimums might also exist but are not considered in this study. To say, we investigate the structure with the strongest interaction energy only. The Ortmann, Bechstedt, and Schmidt (OBS)[31] method is used for dispersion corrections with the PW91 functional method, while the Grimme[32] method is used for dispersion corrections with the PBE functional methods. These methods adopt double precision numerical basis sets that take into account p polarization (DNP) and triple numerical plus polarization (TNP). The sizes of the DNP basis sets are comparable with the 6–31G** basis and are regarded as more accurate than Gaussian basis sets of the same size.[33,34] The energy in each geometry optimization cycle is converged to within $1 \times 10^{-5}$ Hartree with a maximum displacement and force of $5 \times 10^{-3}$ Å and $2 \times 10^{-3}$ Hartree/Å, respectively. The corrections of basis set superposition error (BSSE) evaluated by the counterpoise method for the interaction energy has not been considered, because a recent study has proven that the numerical basis sets implemented in DMol$^3$ can minimize or even eliminate BSSE.[34]

### *Ab initio calculations*

The electron density distribution of ion-$H_2S$ system is calculated using Hartree–Fock method with the Møller–Plesset second-order perturbation (MP2 (Full))[35] energy correction in Gaussian 03[36] at the basis level of 6–311 + + G(d,p). Atoms in molecule (AIM) calculations[37] are carried out using the AIM2000 program.[38]

### *MD simulations*

The NIIL–$H_2S$–$CH_4$ model for MD simulation is constructed with NIILs and fuel gas mixture (10% $H_2S$ and 90% $CH_4$) in cubic simulation boxes. The simulation models are constructed with 100 NIILs, 10 $H_2S$, and 90 $CH_4$ molecules. Molecular relaxation and dynamics are calculated by using Discover module of Materials Studio. An accuracy of $10^{-2}$ kcal/mol is applied to the van der Waals contributions, while the Ewald summation[39] method is invoked to take into account Coulomb interactions. The MD boxes are initially relaxed in NVT ensemble at 298 K for 50 ps, then in NPT ensemble at 298 K and 0.1 MPa for 50 ps, and finally in NVE ensemble for 2000 ps. The Andersen algorithm[40] set to a collision ratio of 1.0 and the Berendsen algorithm[41] set to a decay constant of 0.1 ps are respectively used to control the temperature and pressure of each model. MD simulation is performed using a time step of 1.0 fs for equilibrating the models and obtaining the final structures.

The COMPASS[42,43] (condensed phase optimized molecular potentials for atomistic simulation studies) force field is used to calculate the interaction potential energy. This force field consists of terms for bonds, angles, dihedrals, out-of-plane angles as well as cross-terms, and two nonbonded functions, a Coulombic function for electrostatic interactions and a 9-6 Lennard-Jones potential for van der Waals interactions. It is the first ab initio force field that enables accurate and simultaneous prediction of gas-phase properties and condensed-phase properties. The COMPASS force field has been mainly developed for predicting the structures and dynamics of common organics, inorganic molecules, and polymers, including the ILs.[44,45]

## Results and Discussion

### *Topological characteristics of the cation/anion–$H_2S$ interactions*

The topological properties of the electron density and bond critical points (BCPs) located between hydrogen bond donor and acceptor are characterized by AIM theoretical calculations in each of the cation/anion–$H_2S$ complexes. According to AIM theory, the existence of a chemical bond is characterized by the existence of a $(3, -1)$ type BCP and a bond path, a line of maximum density linking two nuclei and passing the BCP. The nature of chemical bonding is revealed by descriptors at the BCP, such as the electron density ($\rho(r)$) and the Laplacian of electron density ($\nabla^2\rho(r)$).[46,47] In this work, three imidazolium cations and two nonfluorous anions of NIILs are separately investigated for $H_2S$ absorption to find out the possible interaction sites shown in Supporting Information Table S1. The interaction energy values ($\Delta E_{I\text{-}S}$) of ion and $H_2S$ indicate that the $H_2S$ molecule prefers to approach from the S atom toward the $C_2H$ hydrogen for the cation of [bmim] and [hbmim] corresponding to Supporting Information Figure S1(a-4) and (c-4). However, the most stable interaction site of [bhmim] and $H_2S$ is between the $H_2S$ and hydroxyl group on methyl of imidazolium. Then the most stable ion–$H_2S$ systems were used in electron density distribution. The main results of the AIM calculation and the

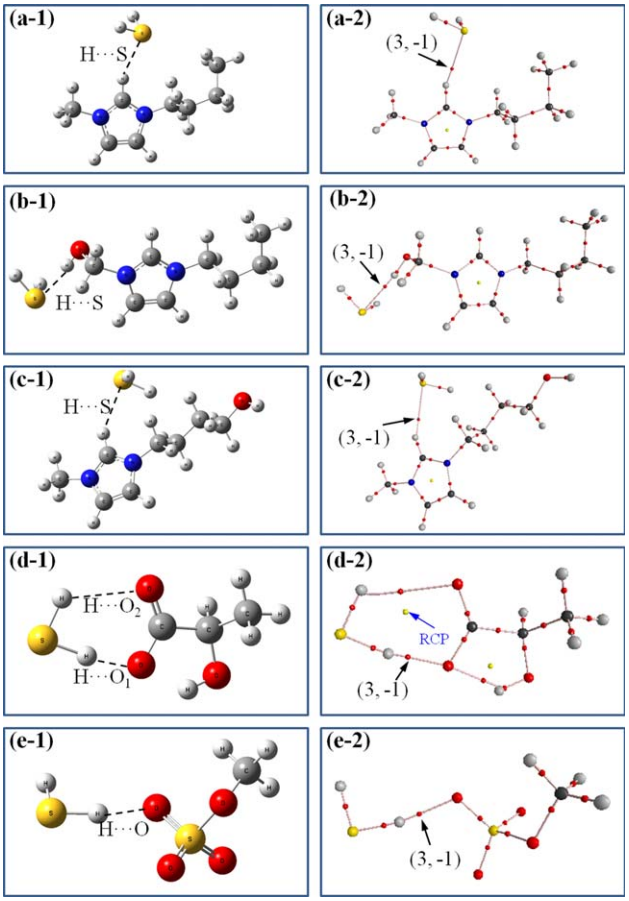


**Figure 1. $H_2S$–ion geometry ((a-1), (b-1), (c-1), (d-1), and (e-1)) calculated at the PW91/DNP theoretical level and AIM analysis for ion–$H_2S$ complexes ((a-2), (b-2), (c-2), (d-2), and (e-2)).**

**Dashed lines in $H_2S$-ion geometry showing possible hydrogen bonds; molecular graphs in AIM analysis with small red dots representing BCP, small yellow dots representing RCP, pink lines representing bond paths, and large dots representing attractors (atoms: black, carbon; gray, hydrogen; red, oxygen; yellow, sulfur): (a-1), (a-2) [bmim]-$H_2S$; (b-1), (b-2) [bhmim]-$H_2S$; (c-1), (c-2) [hbmim]-$H_2S$; (d-1), (d-2) LAC-$H_2S$; (e-1), (e-2) $MeSO_4$-$H_2S$. [Color figure can be viewed in the online issue, which is available at wileyonlinelibrary.com]**

optimized structures are shown in Figure 1. The main hydrogen bond contribution between ion and $H_2S$ from the AIM analysis is given in Table 1. The $\rho(r)$ at BCP correlates with the strength of hydrogen-bonding interaction.[48,49] For the cation–$H_2S$ interactions (Figures 1a–c), the cation with no hydroxyl group ([bmim]) shows the lowest value. For the [bhmim]–$H_2S$ system, the H atom of hydroxyl group acts as the hydrogen bond donor to interact with the S atom of $H_2S$. In the [hbmim]–$H_2S$ system, the S atom of $H_2S$ interacts with the H atom of $C_2H$ hydrogen for the cation. For the anion–$H_2S$ interactions (Figures 1d, e), the values of $\rho(r)$ for both LAC and $MeSO_4$ are higher than those of the cation–$H_2S$ systems. This is attributed to the fact that the two O atoms of carboxylate in LAC interact with the two H atoms of $H_2S$ to form two BCPs and a ring critical point (RCP, (3, +1)). Thus, the electron density of hydrogen-bonding ((3, −1) type BCP (Figure 1 and Table 1) between ion and $H_2S$ increases in the order of: [hbmim], [bmim], [bhmim], $MeSO_4$, and LAC.

The negative Laplacian $\nabla^2\rho(r)$ suggests that the ion–$H_2S$ interaction at the BCP has a covalent character (Table 1). The $\nabla^2\rho(r)$ represents the curvature of the electron density in three-dimensional space.[37] However, the total energy density ($H(r)$, electronic kinetic ($G(r)$) plus potential ($V(r)$) energy density), instead of the Laplacian, is a more appropriate index to better understand the weak nonbonded interaction.[50] As shown in Table 1, the $H(r)$ values of bhmim···$H_2S$ and LAC···$H_2S$ (H···$O_1$) are negative, indicating that the strength of the hydrogen bonding in these systems are strong. Meanwhile, the positive $H(r)$ values of bmin···$H_2S$, hbmim···$H_2S$ and $MeSO_4$···$H_2S$ suggests that H···S of bmin···$H_2S$ and hbmim···$H_2S$, and H···O of $MeSO_4$···$H_2S$ are relatively weaker.

The solubilities of $H_2S$ in these six ILs (Table 2.) have been calculated by the conductor-like screening model for real solvents (COSMO-RS) method,[51] which has been described in detail in Supplementary Information. The high solubility of $H_2S$ in ILs is likely to be ascribed to the hydrogen bond-donor ability of $H_2S$ molecule. The AIM parameters of possible interaction sites (Figure 1, Table 1) allow us to obtain the hydrogen bond properties of the ion–$H_2S$ pairs. The $\rho(r)$ and $H(r)$ results at BCPs of hydrogen bonds from AIM analysis indicate that the strength of hydrogen bond of anion–$H_2S$ interactions are very strong, and that the hydroxyl group attached on the tail of alkyl groups of imidazolium cations is able to influence the $H_2S$ capture capacity. In addition, the anions play a more important role in $H_2S$ capture than cations. Therefore, the topological characteristics of hydrogen bonding between ions and $H_2S$ contribute mainly to the ability of ILs for their $H_2S$ capture.

### *Geometry structure of the NIIL–$H_2S$ system*

As both anion and cation of NIILs can affect their $H_2S$ absorption capacity, an appropriate composition of cations and anions for NIILs will favor the absorption process. Based on the tunable properties of ILs, multiple possible compositions can be achieved for investigation. The optimized structures of absorption products are illustrated in Figure 2 for the six NIIL–$H_2S$ systems, which are different combinations of three imidazolium cations and two nonfluorous anions. The absence of imaginary vibrational frequency confirms that the structure of absorption product corresponds to a true minimum.

**Table 1. AIM Parameters (in atomic units) of Main Hydrogen Bonds in Ion–$H_2S$ Complexes Corresponding to Figure 1**

| Ion–$H_2S$ pairs | $\rho(r)$ | $\nabla^2\rho(r)$ | $G(r)$ | $V(r)$ | $H(r)$ |
|---|---|---|---|---|---|
| bmin···$H_2S$ (H···S) | 0.0132 | − 0.0092 | 0.0077 | − 0.0062 | 0.0015 |
| bhmim···$H_2S$ (H···S) | 0.0308 | − 0.0164 | 0.0190 | − 0.0217 | − 0.0027 |
| hbmim···$H_2S$ (H···S) | 0.0123 | − 0.0087 | 0.0073 | − 0.0059 | 0.0014 |
| LAC···$H_2S$ (H···$O_1$) | 0.0460 | − 0.0341 | 0.0377 | − 0.0412 | − 0.0035 |
| LAC···$H_2S$ (H···$O_2$) | 0.0079 | − 0.0067 | 0.0059 | − 0.0052 | 0.0007 |
| LAC···$H_2S$ (RCP) | 0.0069 | − 0.0077 | 0.0064 | − 0.0051 | 0.0013 |
| $MeSO_4$···$H_2S$ (H···O) | 0.0324 | − 0.0296 | 0.0281 | − 0.0267 | 0.0014 |

**Table 2.. The Henry's Law Constants of $H_2S$ in the Imidazolium-based ILs at 298.15 K Predicted by COSMO-RS**

| ILs | $K_H$ (mol/(L·atm)) |
|---|---|
| [bmim]$MeSO_4$ | 1.0289 |
| [bmim]LAC | 0.9344 |
| [bhmim]$MeSO_4$ | 0.6353 |
| [bhmim]LAC | 0.6018 |
| [hbmim]$MeSO_4$ | 0.7931 |
| [hbmim]LAC | 0.7582 |

Figure 2 shows that anions, that is, $MeSO_4$ and LAC, provide the main interaction sites to capture $H_2S$. The interaction of ion pairs of NIILs is based on the electrostatic force and hydrogen bonding between different cations and anions.[52] The geometry structures of NIILs were optimized by the DFT-D methods (Supporting Information Figure S2), and the calculated cation–anion interaction energy ($\Delta E_{A-C}$) is shown in Supporting Information Table S3. The results indicate that the anion takes the more negative energy from its most electronegative atoms toward the acidic $C_2H$ hydrogen of the imidazolium cation than toward the hydrogen atoms of the side chain, which is consistent with the previous investigations.[53,54]

The interactions of $H_2S$ with ion pairs of NIILs are all analyzed through the anions with the H···O hydrogen bond as shown in Figure 2. The hydrogen bonds are formed between hydrogen atom and the acceptor atom with one lone electron pair at least. The distance between the hydrogen atom and the acceptor is less than or equal to the maximum hydrogen–acceptor distance (2.5 Å in this work). The van der Waals radii of H and O atoms are 1.09 and 1.52 Å, respectively.[55] Such a maximum distance is specified to obtain the relative strong hydrogen bond in this $H_2S$ capture system. If both the hydrogen and acceptor atoms are within the same molecule, they are separated by at least four nearest neighbor shells. The H atom of $H_2S$ acts as the hydrogen bond donor, and the O atom of $MeSO_4$ or LAC as the hydrogen bond acceptor. For [hbmim]LAC–$H_2S$ and [hbmim]$MeSO_4$–$H_2S$ systems, another hydrogen bond for capturing $H_2S$ exists between the H atom of hydroxyl group in imidazolium ring and the S atom of $H_2S$. Thus, the hydrogen bonding may play an important part in the geometry structure of NIIL–$H_2S$ systems. In addition, for the same anion, LAC, the NIIL that contains imidazolium cation with *n*-hydroxybutyl group shows a shorter distance between the H atom in $H_2S$ and the O atom in anion, thus giving rise to an effective interaction. In the case of the same cation, the NIIL with LAC has the

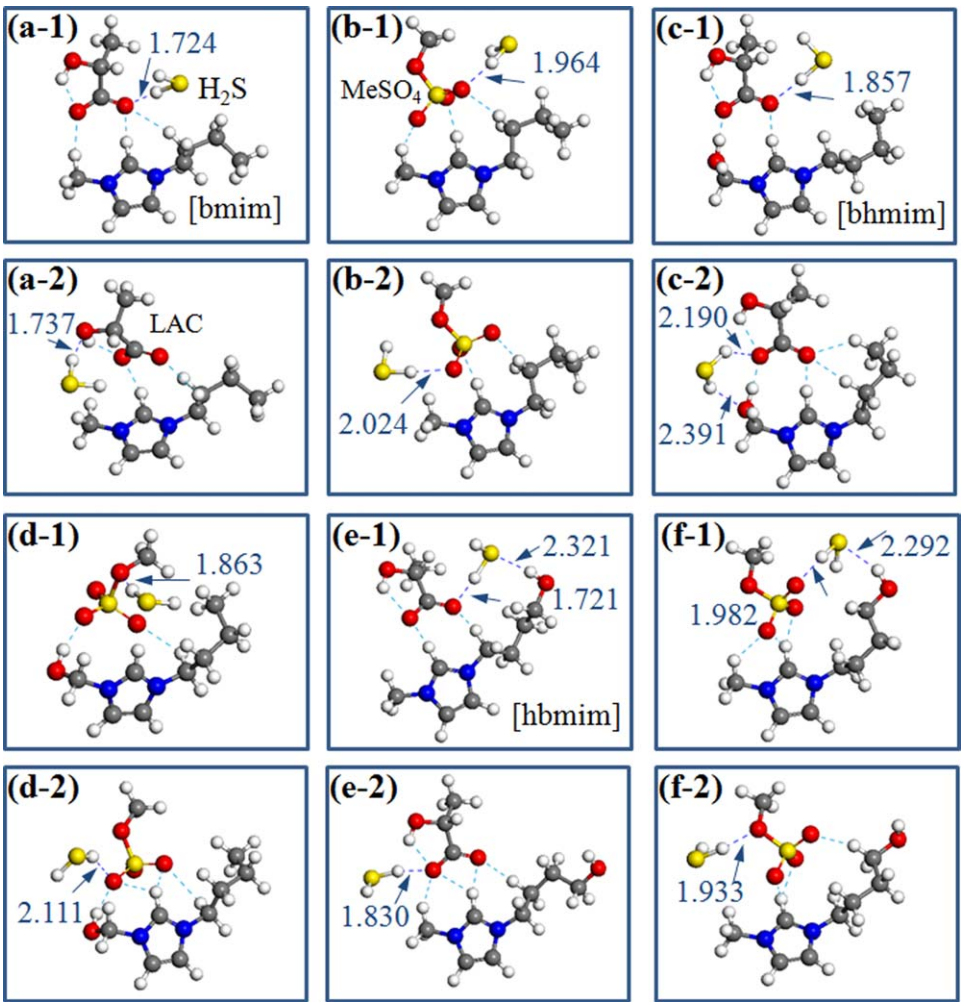


**Figure 2. Geometry structures of NIILs for different $H_2S$ sites relative to NIILs with the hydrogen bond length in Angstrom and the interaction energy shown in Table S4.**

**[Color figure can be viewed in the online issue, which is available at wileyonlinelibrary.com]**

shorter distance of hydrogen bond. In practice, ion pairs of NIILs have been applied to treat fuel gas and many industrial waste gas streams. Thus, the interaction performance of the ion pairs and $H_2S$ is essential in task-specific IL design and exploration.

### *NIILs–$H_2S$/$CH_4$ interaction energy*

The interaction energy ($\Delta E_{IL\text{-}S}$) between the NIIL and $H_2S$ reflects the strength and stabilization of $H_2S$ sequestering by NIILs through hydrogen bonds.[13] The $\Delta E_{IL\text{-}S}$ (in kcal/mol) of NIIL–$H_2S$ systems can be calculated as

$$\Delta E = 2625.46[E_{NIIL-H_2S} - (E_{NIIL} - E_{H_2S})] \quad (1)$$

where $E_{NIIL-H_2S}$ (Hatree) is the energy of absorption system, and $E_{NIIL}$ (Hatree) and $E_{H_2S}$ (Hatree) are the energies of the NIIL and $H_2S$, respectively. The interaction energy ($\Delta E_{IL\text{-}M}$) between the NIIL and $CH_4$ can be calculated by using the same method with the energies of $E_{NIIL-CH_4}$ and $E_{CH_4}$ (Hatree).

The interactions of NIILs and $H_2S$ or $CH_4$ molecules were calculated by using the most stable structure of NIILs from Supporting Information Figure S2 (a-2∼f-2), and the interaction energy ($\Delta E_{IL\text{-}S}$) for different $H_2S$ sites relative to NIILs are shown in Supporting Information Table S4 with the corresponding geometry structures in Figure 2. The possible absorption sites of $CH_4$ were the same with those of $H_2S$ shown in Supporting Information Figure S3 with the interaction energy in Supporting Information Table S5. The $\Delta E_{IL\text{-}S}$ and $\Delta E_{IL\text{-}M}$ of more stable adsorption structures obtained from Supporting Information Tables S4 and S5 are shown in Figure 3. The negative values indicate that the systems tend to be stable with the absorption of gases. For LAC anion, the NIIL with the cation containing the hydroxyl on the tail of *n*-butyl ([hbmim]) gives the lowest $\Delta E_{IL\text{-}S}$ value of $-15.805$ kcal/mol. However, the NIIL with the [bmim] cation has a lowest $\Delta E_{IL\text{-}S}$ for $MeSO_4$ anion. As the interaction energy between anion and cation increases, the free volume

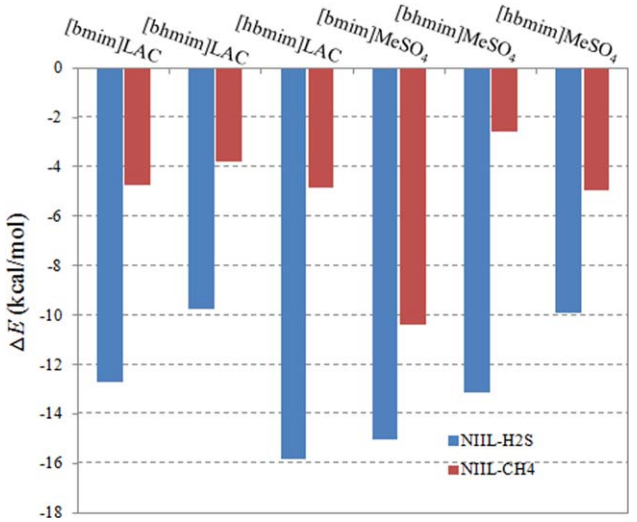


**Figure 3. Interaction energy ($\Delta E_{A-C}$) of anion and cation in NIILs with the most stable geometry structures corresponding to Figure S2 (a-2~f-2) with the anion toward the most acidic hydrogen atom in the imidazolium ring.**

**[Color figure can be viewed in the online issue, which is available at wileyonlinelibrary.com]**

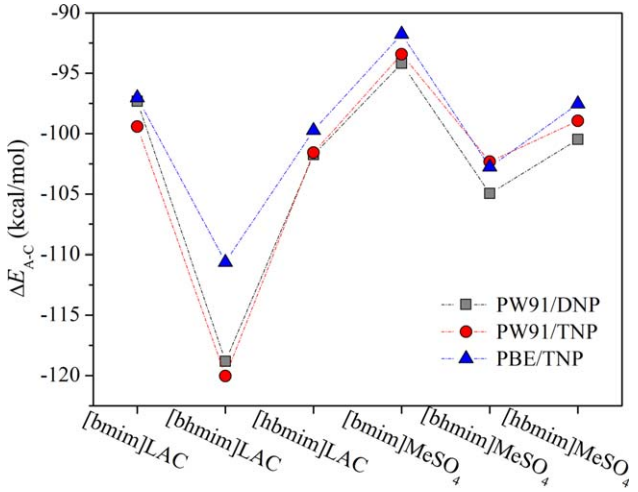


**Figure 4. Interaction energy ($\Delta E_{IL\text{-}S}$/$\Delta E_{IL\text{-}M}$) between NIIL and $H_2S$/$CH_4$ with more stable adsorption structure calculated at PBE/TNP basis level from DFT-D methods.**

**[Color figure can be viewed in the online issue, which is available at wileyonlinelibrary.com]**

or void volume decreases, giving rise to accessibility of less space to accommodate the solute molecules. The [bhmim]-LAC presents the largest absolute value of $\Delta E_{A-C}$ in Figure 4. These results indicate that [bhmim]LAC has the least free volume to sequester $H_2S$. Thus, $\Delta E_{IL\text{-}S}$ in Figure 3 indicate that [bhmim]LAC presents the weak interaction with the lowest absolute value of $\Delta E_{IL\text{-}S}$.

The $\Delta E_{IL\text{-}S}$ and the geometry characteristics indicate that cations also play a role in acid gas absorption (Figure 3). This is in agreement with both experimental results[11,12] and theoretical calculations.[17,49] The hydrogen bond has a strong orientation dependence, as the highly orientation dependent electrostatic interaction is the main source of the attraction in the hydrogen bond.[56] The QC calculations demonstrate that these six NIILs are efficient solvents for separation of $H_2S$ from $CH_4$ from more negative values of $\Delta E_{IL\text{-}S}$ than those of $\Delta E_{IL\text{-}M}$. [hbmim]LAC with the largest difference between $\Delta E_{IL\text{-}S}$ and $\Delta E_{IL\text{-}M}$ might be the best NIILs for selectively capturing $H_2S$ from the $H_2S$–$CH_4$ mixture. However, $[bmim]MeSO_4$ with the smallest difference between the interaction energy shows the poorest separation efficiency. Furthermore, the structure diversity of cation and anion, such as the alkyl chain and hydroxyl group in the imidazolium cation, and the electronegative atoms of anions, leads to different $H_2S$ capture properties of NIILs.

### *Microstructural features of the NIIL–$H_2S$/$CH_4$ system*

MD simulations are performed for the NIIL–$H_2S$–$CH_4$ systems under isobaric (0.1 MPa) and isothermal (298 K) conditions. Microscopic distributions of the system are usually represented by radial distribution functions (RDFs), which reflect the organization of $H_2S$ around cations or anions. In a real system, $CH_4$ is the main component of fuel gas, and an effective absorption solution should selectively capture low-concentration $H_2S$ from the gas mixture. Thus, to simulate the real situation, a gas mixture containing 10% $H_2S$ and 90% $CH_4$ is chosen. Figure 5 shows the site–site RDFs (g(r)) of the NIIL–$H_2S$ systems, including the main interaction sites obtained in QC calculations for each system

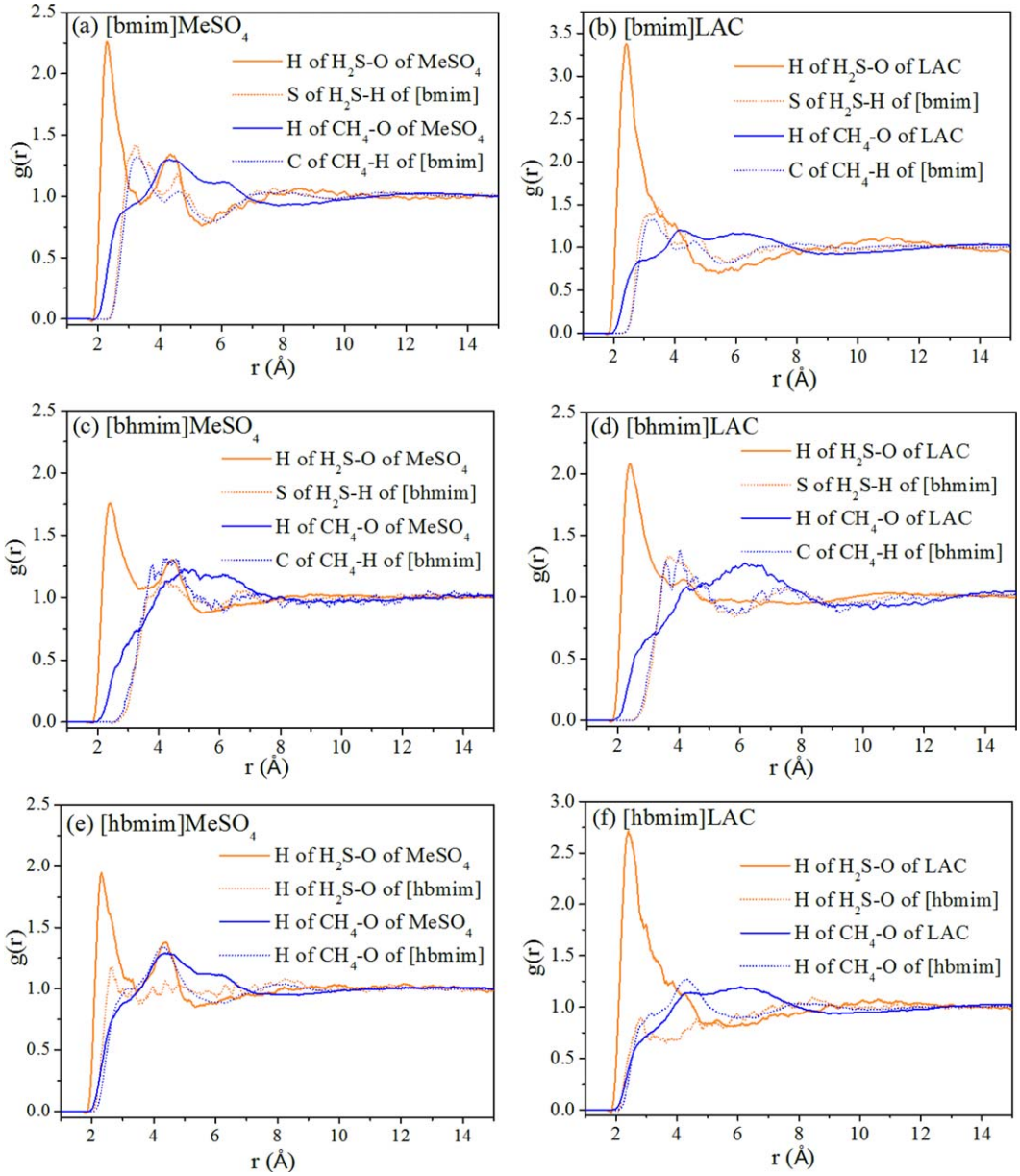


**Figure 5. Site-site radial distribution functions (RDFs) of the systems of NIIL and the mixed gas (10% $H_2S$ and 90% $CH_4$) at 298.15 K and 0.1 MPa obtained from molecular dynamics simulations.**

**(a) [bmim]$MeSO_4$; (b) [bmim]LAC; (c) [bhmim]$MeSO_4$; (d) [bhmim]LAC; (e) [hbmim]$MeSO_4$; and (f) [hbmim]LAC. The interaction sites in RDF analysis according to the results in Figure 1 obtained from DFT-D calculations. [Color figure can be viewed in the online issue, which is available at wileyonlinelibrary.com]**

(BCPs in Figure 1). The possible site–site RDFs of the NIIL–$CH_4$ system are also calculated for comparison with the NIIL–$H_2S$ systems.

The highest RDF values are obtained for the $H_2S$–anion interactions in the ion pair systems, which is in agreement with the results of other works for acidic gas and conventional IL interactions.[9,57] The distance in the maximum probability between the H of $H_2S$ and the O of $MeSO_4$ or LAC (BCPs in Figure 1, Table 1) is characterized by a sharp, intense peak around 2.5 Å. It is the distance for the first coordination shells of $H_2S$ molecules around the anions. However, the distance between the H of $CH_4$ and the O of $MeSO_4$ or LAC is longer than that of the $H_2S$–anion system, which is in the range of 4–5 Å. This indicates that interactions between $CH_4$ and anions are relatively weaker. The $MeSO_4$ anion in the three NIILs has the second coordination shell of $H_2S$ (about 4.3 Å), which is not true for the NIILs with LAC anion.

The RDFs for $H_2S$-cations and $CH_4$-cations are almost the same, except for the [hbmim] cation, showing the weak peaks. The distance in the maximum probability between the H atom of $H_2S$ and the O atom of hydroxyl in [hbmim] is around 2.6 Å, shorter than $CH_4$–[hbmim] (about 4.2 Å). This reveals that the imidazolium cation with *n*-hydroxybutyl group in NIIL can interact with $H_2S$ molecules, together with anions, and enhance its $H_2S$-capturing ability.

Microstructural features of NIIL–$H_2S$ systems suggest that anions have the closest affinity with $H_2S$, which is consistent with the results of electron density at BCPs in this work. The RDFs characteristics of anions and $H_2S$ in absorption

systems show sharp peaks at the distance of 2.5 Å (Figure 5), suggesting the strong interactions between $H_2S$ and anions. The $H_2S$ molecules around the $MeSO_4$ (Figures 5a, c, and e) shows two possible coordination shells, and $CH_4$ only appears at the second coordination shell or further away, demonstrating the weak interactions between NIIL and $CH_4$ pairs. Such different RDF characteristics are likely to explain the fact that $CH_4$ is poorly absorbed in ILs,[58] and that NIIL is able to selectively absorb low-concentration $H_2S$ from the $H_2S$–$CH_4$ mixture.

### *Dynamics of $H_2S$, $CH_4$, and ion pairs*

The dynamic nature of the NIIL–$H_2S$ system is characterized through exploring the center-of-mass (COM) mean square displacements (MSDs) of $H_2S$, $CH_4$, cations, and anions as a function of time. The self-diffusion coefficients of components in the NIIL–$H_2S$ systems can be calculated with the Einstein equation[59]

$$D = \frac{1}{6N_\alpha} \lim_{t\to\infty} \frac{d}{dt} \sum_{i=1}^{N_\alpha} \langle [r_i(t) - r_i(0)]^2 \rangle \qquad (2)$$

where $r_i(t) - r_i(0)$ is the (vector) distance traveled by the population of atoms of type $i$ over a time interval $t$. The square of the magnitude of this vector is averaged over rolling time intervals. The quantity in bracket represents the MSD.

Table 3 shows the linear regression equation of total COM MSD ($m$ in Å$^2$) versus time ($t$ in ps) for six NIILs with various combinations of three cations and two anions containing $H_2S$ and $CH_4$. Total COM MSD values are the sum of the individual $x$, $y$, and $z$ COM MSD contributions. A linear relationship of log(MSD) against log(time) is obtained (Supporting Information Figure S4), indicating that the calculation results are reliable. The MSDs for these systems are in a linear relationship with time, thus, their self-diffusion coefficients for the components could be obtained by fitting the slope of this linear region (Table 3). The MSDs of $CH_4$ and $H_2S$ are higher than those of cations and anions for all the NIIL–$H_2S$ systems, indicating the greater diffusive motion of the former species than the latter two.

The self-diffusion coefficients of $H_2S$ and $CH_4$ (Figure 6a) in the six NIIL–$H_2S$–$CH_4$ systems differ substantially with the different cations and anions. For the $MeSO_4$ anion, the self-diffusion coefficients of $H_2S$ and $CH_4$ in NIIL with [bhmim] are larger than the other systems. However, those of gases in NIIL with [hbmim] show the smallest values. The diffusion coefficients of NIILs are calculated from $D_{NIIL} = 0.5(D_{cation} + D_{anion})$. Figure 6b shows the diffusion coefficients of NIILs and the cations and anions in the six NIIL–$H_2S$–$CH_4$ systems. For the NIIL with the same cation of [bmim], the diffusion coefficients of cation are higher than those of the anions. However, for the NIIL with the same cation of [bhmim], the cations exhibit lower diffusion coefficients than the anions. For the NIIL with the same cation of [hbmim], the diffusion coefficients of cations are of almost the same level with the anions. The diffusion coefficients of these species might be associated with the viscosity of NIILs. The viscosity of NIILs is related to the cation–anion pairing and their structural characteristics, such as cationic size, length of substituted group, flexible ether oxygen on alkyl chain, anionic size, and anionic shape, etc.[60–63] The low viscosity is ascribed to the less rigid characteristics and more conformational degrees of freedom.[60,64] The high diffusion coefficient of [bhmim]$MeSO_4$ might be attributed to the fact that the hydroxyl on the methyl group of imidazolium increases the conformational degrees of freedom for the cation, and decreases the viscosity with high diffusion coefficients. The hydrogen bonding of the hydroxyl group on the short alkyl group (methyl) could be weakened by the steric effects. Moreover, the composition and size of anion may substantially affect the diffusion coefficients.[65] However, this warrants a further experimental and simulation investigation. In addition, the diffusion coefficients of $H_2S$ are lower than those of $CH_4$ in most NIILs, indicating the stronger interaction between $H_2S$ and NIILs with a higher rate of their absorption in the NIILs. This further indicates that the NIILs

**Table 3. Diffusion Coefficient ($D$) of $H_2S$, $CH_4$, Cations and Anions in the NIIL–$H_2S$–$CH_4$ Systems at Ambient Temperature (298 K) and Atmosphere Pressure (0.1 MPa)**

| System | | Linear regression equation $m$ (Å$^2$), $t$ (ps) | $R^2$ | $D$ ($10^{-6}$ cm$^2$/s) |
|---|---|---|---|---|
| [bmim]$MeSO_4$ | $H_2S$ | $m = 0.5823t - 79.1915$ | 0.9743 | 9.71 |
| | $CH_4$ | $m = 0.5840t + 23.1621$ | 0.9991 | 9.73 |
| | Cation | $m = 0.0669t + 6.2070$ | 0.9974 | 1.12 |
| | Anion | $m = 0.0481t + 4.8140$ | 0.9924 | 0.80 |
| [bmim]LAC | $H_2S$ | $m = 0.4183t + 0.0835$ | 0.9939 | 6.97 |
| | $CH_4$ | $m = 0.5177t + 8.1073$ | 0.9989 | 8.63 |
| | Cation | $m = 0.0770t + 7.4853$ | 0.9967 | 1.28 |
| | Anion | $m = 0.0277t + 7.4916$ | 0.9893 | 0.46 |
| [bhmim]$MeSO_4$ | $H_2S$ | $m = 2.5579t + 26.3792$ | 0.9990 | 42.63 |
| | $CH_4$ | $m = 3.3889t + 40.5429$ | 0.9902 | 56.48 |
| | Cation | $m = 0.2396t + 18.9532$ | 0.9979 | 3.99 |
| | Anion | $m = 0.3154t + 9.3525$ | 0.9991 | 5.26 |
| [bhmim]LAC | $H_2S$ | $m = 0.3245t + 36.5719$ | 0.9826 | 5.41 |
| | $CH_4$ | $m = 0.2483t + 21.4682$ | 0.9970 | 4.14 |
| | Cation | $m = 0.0203t + 6.4025$ | 0.9830 | 0.34 |
| | Anion | $m = 0.0260t + 3.2211$ | 0.9601 | 0.43 |
| [hbmim]$MeSO_4$ | $H_2S$ | $m = 0.3044t + 24.6139$ | 0.9908 | 5.07 |
| | $CH_4$ | $m = 0.3889t + 21.6150$ | 0.9982 | 6.48 |
| | Cation | $m = 0.0233t + 3.2092$ | 0.9975 | 0.39 |
| | Anion | $m = 0.0222t + 1.5353$ | 0.9691 | 0.37 |
| [hbmim]LAC | $H_2S$ | $m = 0.3980t + 40.0547$ | 0.9907 | 6.63 |
| | $CH_4$ | $m = 0.4709t + 9.7230$ | 0.9986 | 7.85 |
| | Cation | $m = 0.0248t + 6.6086$ | 0.9913 | 0.41 |
| | Anion | $m = 0.0242t + 4.6067$ | 0.9915 | 0.40 |

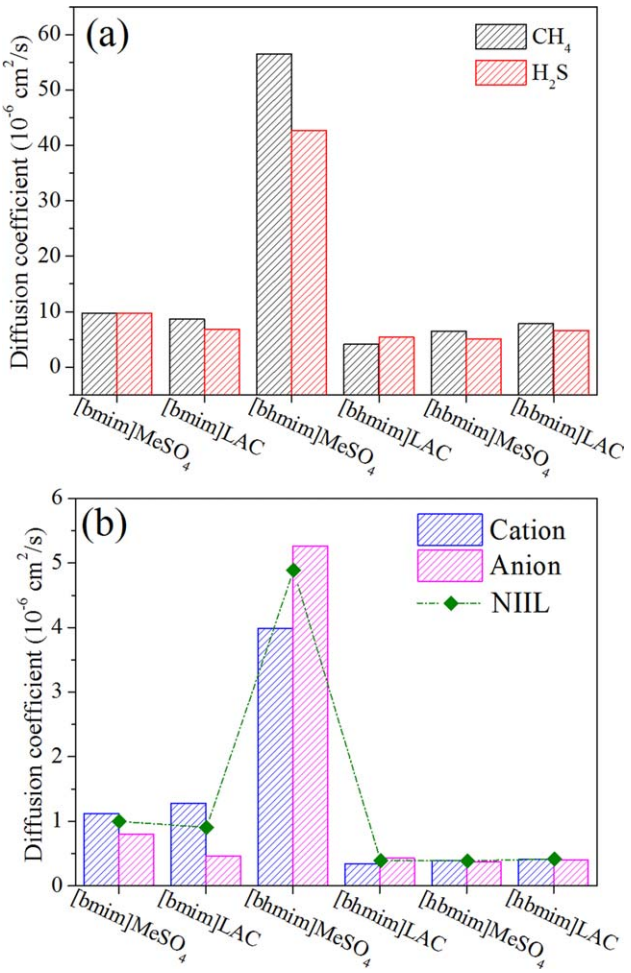


**Figure 6. Diffusion coefficients of (a) $H_2S$ and $CH_4$; and (b) cation, ion and NIIL in the NIIL-$H_2S$-$CH_4$ systems.**

**[Color figure can be viewed in the online issue, which is available at wileyonlinelibrary.com]**

could be used to selectively capture $H_2S$ from the $H_2S$–$CH_4$ mixture.

The dynamic nature of the NIIL–$H_2S$–$CH_4$ system shows that the MSDs of cations and anions over time are of a similar magnitude for the NIILs with the cations of [bhmim] and [hbmim] (Supporting Information Figure S4). This suggests that ion pairs in the NIILs with hydroxyl group cations have important interactions. The self-diffusion coefficients of all the species in the NIIL–$H_2S$–$CH_4$ systems differ with the compositions of the cation and anion, leading to their different $H_2S$ capture properties.

## Conclusions

In this work, NIILs with different combinations of imidazolium cations and nonfluorous anions are explored for selectively removing $H_2S$ from binary gas mixture. The effective absorption sites, structural features, and the diffusivities of gases in the NIILs are successfully identified. The effective interaction sites of ions with $H_2S$ obtained from the QC calculations suggest that hydrogen bonding is the main force for NIIL as the promising alternative to capture $H_2S$. The alkyl chain and hydroxyl group in the imidazolium cation, and the electronegative atoms of anions, influence their $H_2S$ capture capacities. MD simulations reveal that the imidazolium with *n*-hydroxybutyl group on the tail of long alkyl chain can more effectively interact with $H_2S$ molecules, together with anions, and enhance its $H_2S$-capturing ability. Furthermore, the QC calculation results show that [hbmim]-LAC has the largest interaction energy with $H_2S$ molecule. Thus, [hbmim]LAC might be the best NIILs for selectively capturing $H_2S$ from the $H_2S$–$CH_4$ mixture from molecular modeling. The tunable combinations of cations and anions in NIILs have significant impacts on $H_2S$ capture. This study gives an insight into the interactions between $H_2S$ and NIILs, and has implications for designing and developing new NIILs for practical applications.


## Acknowledgments

The authors wish to thank the Fundamental Research Funds for the Central Universities (WK2060190007) for the partial support of this study. The numerical calculations in this work have been performed on the supercomputing system in the Supercomputing Center of University of Science and Technology of China.


## Notation

LAC = lactate anion
$MeSO_4$ = methylaulfate anion
[bmim] = 1-*n*-butyl-3-methylimidazolium
[bhmim] = 1-*n*-butyl-3-hydroxymethyl-imidazolium
[hbmim] = 1-*n*-hydroxybutyl-3-methyl-imidazolium
NIIL = nonfluorous imidazolium ionic liquid
QC = quantum chemistry
DFT-D = density functional theory with dispersion correction
MD = molecular dynamics
AIM = atoms in molecule
BCP = bond critical point
$\rho(r)$ = electron density
$\nabla^2\rho(r)$ = Laplacian of electron density
RCP = ring critical point
$H(r)$ = total energy density
$G(r)$ = electronic kinetic energy density
$V(r)$ = electronic potential energy density
$\Delta E_{I\text{-}S}$ = interaction energy of ion (anion or cation) and $H_2S$
$\Delta E_{A-C}$ = interaction energy of anion and cation in NIIL
$\Delta E_{IL\text{-}S}$ = interaction energy of NIIL and $H_2S$
$\Delta E_{IL\text{-}M}$ = interaction energy of NIIL and $CH_4$
RDF ($g(r)$) = radial distribution function
COM = center-of-mass
MSD = mean square displacement

## Literature Cited


1. Kohl AL, Nielsen RB. Gas Purification, 5th ed. Texas: Gulf Publishing Company, 1997.
2. Guo B, Duan E, Zhong Y, Gao L, Zhang X, Zhao D. Absorption and oxidation of $H_2S$ in caprolactam tetrabutyl ammonium bromide ionic liquid. *Energy Fuels*. 2011;25(1):159–161.
3. Gabriel D, Deshusses MA. Retrofitting existing chemical scrubbers to biotrickling filters for $H_2S$ emission control. *Proc Natl Acad Sci USA*. 2003;100(11):6308–6312.
4. Ma X, Wang X, Song C. "Molecular basket" sorbents for separation of $CO_2$ and $H_2S$ from various gas streams. *J Am Chem Soc*. 2009;131(16):5777–5783.
5. Ros A, Lillo-Ródenas MA, Canals-Batlle C, Fuente E, Montes-Morán MA, Martin MJ, Linares-Solano A. A new generation of sludge-based adsorbents for $H_2S$ abatement at room temperature. *Environ Sci Technol*. 2007;41(12):4375–4381.
6. Song J, Luo Z, Britt DK, Furukawa H, Yaghi OM, Hardcastle KI, Hill CL. A multiunit catalyst with synergistic stability and reactivity: a polyoxometalate-metal organic framework for aerobic decontamination. *J Am Chem Soc*. 2011;133(42):16839–16846.

7. Mandal B, Bandyopadhyay SS. Simultaneous absorption of $CO_2$ and $H_2S$ into aqueous blends of N-methyldiethanolamine and diethanolamine. *Environ Sci Technol*. 2006;40(19):6076–6084.
8. Rochelle GT. Amine scrubbing for $CO_2$ capture. *Science*. 2009;325 (5948):1652–1654.
9. Aparicio S, Atilhan M. Computational study of hexamethylguanidinium lactate ionic liquid: a candidate for natural gas sweetening. *Energy Fuels*. 2010;24(9):4989–5001.
10. Brennecke JF, Maginn EJ. Ionic liquids: innovative fluids for chemical processing. *AIChE J*. 2001;47(11):2384–2389.
11. Jalili AH, Rahmati-Rostami M, Ghotbi C, Hosseini-Jenab M, Ahmadi AN. Solubility of $H_2S$ in ionic liquids [bmim][$PF_6$], [bmim][$BF_4$], and [bmim][$Tf_2N$]. *J Chem Eng Data*. 2009;54(6):1844–1849.
12. Rahmati-Rostami M, Ghotbi C, Hosseini-Jenab M, Ahmadi AN, Jalili AH. Solubility of $H_2S$ in ionic liquids [hmim][$PF_6$], [hmim][$BF_4$], and [hmim][$Tf_2N$]. *J Chem Thermodyn*. 2009;41(9):1052–1055.
13. Pomelli CS, Chiappe C, Vidis A, Laurenczy G, Dyson PJ. Influence of the interaction between hydrogen sulfide and ionic liquids on solubility: experimental and theoretical investigation. *J Phys Chem B*. 2007;111(45):13014–13019.
14. Heintz YJ, Sehabiague L, Morsi BI, Jones KL, Luebke DR, Pennline HW. Hydrogen sulfide and carbon dioxide removal from dry fuel gas streams using an ionic liquid as a physical solvent. *Energy Fuels*. 2009;23(10):4822–4830.
15. Hernández-Fernández FJ, de los Ríos AP, Gómez D, Rubio M, Víllora G. Selective extraction of organic compounds from transesterification reaction mixtures by using ionic liquids. *AIChE J*. 2010;56(5):1213–1217.
16. Anantharaj R, Banerjee T. Quantum chemical studies on the simultaneous interaction of thiophene and pyridine with ionic liquid. *AIChE J*. 2011;57(3):749–764.
17. Dang LX, Wick CD. Anion effects on interfacial absorption of gases in ionic liquids. *A molecular dynamics study*. *J Phys Chem B*. 2011;115(21):6964–6970.
18. Cadena C, Anthony JL, Shah JK, Morrow TI, Brennecke JF, Maginn EJ. Why is $CO_2$ so soluble in imidazolium-based ionic liquids? *J Am Chem Soc*. 2004;126(16):5300–5308.
19. Wasserscheid P, van Hal R, Bösmann A, Eber J, Jess A. New ionic liquids based on alkylsulfate and alkyl oligoether sulfate anions: synthesis and applications. In: Rogers RD, Seddon KR, editors. Ionic Liquids as Green Solvents. Vol. 856. Washington, DC: American Chemical Society (ACS), 2003:57–69.
20. Davis JJH, Fox PA. From curiosities to commodities: ionic liquids begin the transition. *Chem Commun*. 2003(11):1209–1212.
21. Swatloski RP, Holbrey JD, Rogers RD. Ionic liquids are not always green: hydrolysis of 1-butyl-3-methylimidazolium hexafluorophosphate. *Green Chem*. 2003;5(4):361–363.
22. Shiflett MB, Niehaus AMS, Yokozeki A. Separation of $CO_2$ and $H_2S$ using room-temperature ionic liquid [bmim][$MeSO_4$]. *J Chem Eng Data*. 2010;55(11):4785–4793.
23. Wasserscheid P, van Hal R, Bösmann A. 1-n-Butyl-3-methylimidazolium ([bmim]) octylsulfate-an even 'greener' ionic liquid. *Green Chem*. 2002;4(4):400–404.
24. Zhang J, Zhang S, Dong K, Zhang Y, Shen Y, Lv X. Supported absorption of $CO_2$ by tetrabutylphosphonium amino acid ionic liquids. *Chem Eur J*. 2006;12(15):4021–4026.
25. Ma JW, Zhou Z, Zhang F, Fang CG, Wu YT, Zhang ZB, Li AM. Ditetraalkylammonium amino acid ionic liquids as $CO_2$ absorbents of high capacity. *Environ Sci Technol*. 2011;45(24):10627–10633.
26. Bates ED, Mayton RD, Ntai I, Davis JH Jr. $CO_2$ capture by a task-specific ionic liquid. *J Am Chem Soc*. 2002;124(6):926–927.
27. Yu GR, Zhao DC, Wen L, Yang SD, Chen XC. Viscosity of ionic liquids: database, observation, and quantitative structure–property relationship analysis. *AIChE J*. 2012;58(9):2885–2899.
28. Bhargava BL, Krishna AC, Balasubramanian S. Molecular dynamics simulation studies of $CO_2$-[bmim][$PF_6$] solutions: effect of $CO_2$ concentration. *AIChE J*. 2008;54(11):2971–2978.
29. Perdew JP, Chevary JA, Vosko SH, Jackson KA, Pederson MR, Singh DJ, Fiolhais C. Atoms, molecules, solids, and surfaces – applications of the generalized gradient approximation for exchange and correlation. *Phys Rev B*. 1992;46(11):6671–6687.
30. Delley B. From molecules to solids with the $DMol^3$ approach. *J Chem Phys*. 2000;113(18):7756–7764.
31. Ortmann F, Bechstedt F, Schmidt WG. Semiempirical van der Waals correction to the density functional description of solids and molecular structures. *Phys Rev B*. 2006;73(20):205101.
32. Grimme S. Semiempirical GGA-type density functional constructed with a long-range dispersion correction. *J Comput Chem*. 2006; 27(15):1787–1799.
33. Bald I, Wang YG, Dong M, Rosen CB, Ravnsbaek JB, Zhuang GL, Gothelf KV, Wang JG, Besenbacher F. Control of self-assembled 2D nanostructures by methylation of guanine. *Small*. 2011;7(7):939–949.
34. Inada Y, Orita H. Efficiency of numerical basis sets for predicting the binding energies of hydrogen bonded complexes: evidence of small basis set superposition error compared to Gaussian basis sets. *J Comput Chem*. 2008;29(2):225–232.
35. Head-Gordon M, Pople JA, Frisch MJ. MP2 energy evaluation by direct methods. *Chem Phys Lett*. 1988;153(6):503–506.
36. Frisch MJ, Trucks GW, Schlegel HB, Scuseria GE, Robb MA, Cheeseman JR, Montgomery JA Jr, Vreven T, Kudin KN, Burant JC, Millam JM, Iyengar SS, Tomasi J, Barone V, Mennucci B, Cossi M, Scalmani G, Rega N, Petersson GA, Nakatsuji H, Hada M, Ehara M, Toyota K, Fukuda R, Hasegawa J, Ishida M, Nakajima T, Honda Y, Kitao O, Nakai H, Klene M, Li X, Knox JE, Hratchian HP, Cross JB, Adamo C, Jaramillo J, Gomperts R, Stratmann RE, Yazyev O, Austin AJ, Cammi R, Pomelli C, Ochterski JW, Ayala PY, Morokuma K, Voth GA, Salvador P, Dannenberg JJ, Zakrzewski VG, Dapprich S, Daniels AD, Strain MC, Farkas O, Malick DK, Rabuck AD, Raghavachari K, Foresman JB, Ortiz JV, Cui Q, Baboul AG, Clifford S, Cioslowski J, Stefanov BB, Liu G, Liashenko A, Piskorz P, Komaromi I, Martin RL, Fox DJ, Keith T, Al-Laham MA, Peng CY, Nanayakkara A, Challacombe M, Gill PMW, Johnson B, Chen W, Wong MW, Gonzalez C, Pople JA. Gaussian 03, Revision B.02. Pittsburgh, PA: Gaussian, Inc., 2003.
37. Bader RFW. Atoms in Molecules: A Quantum Theory. Oxford: Oxford University Press, 1990.
38. Biegler-Konig F, Schonbohm J, Bayles D. AIM2000 – a program to analyze and visualize atoms in molecules. *J Comput Chem*. 2001;22(5):545–559.
39. Essmann U, Perera L, Berkowitz ML, Darden T, Lee H, Pedersen LG. A smooth particle mesh Ewald method. *J Chem Phys*. 1995; 103(19):8577–8593.
40. Andersen HC. Molecular dynamics simulations at constant pressure and/or temperature. *J Chem Phys*. 1980;72(4):2384–2393.
41. Berendsen HJC, Postma JPM, Vangunsteren WF, Dinola A, Haak JR. Molecular dynamics with coupling to an external bath. *J Chem Phys*. 1984;81(8):3684–3690.
42. Sun H. COMPASS: an ab initio force-field optimized for condensed-phase applications – overview with details on alkane and benzene compounds. *J Phys Chem B*. 1998;102(38):7338–7364.
43. Sun H, Ren P, Fried JR. The COMPASS force field: parameterization and validation for phosphazenes. *Comput Theor Polym Sci*. 1998;8(1–2):229–246.
44. Bai XT, Gao YA, Liu HG, Zheng LQ. Synthesis of amphiphilic ionic liquids terminated gold nanorods and their superior catalytic activity for the reduction of nitro compounds. *J Phys Chem C*. 2009;113(41):17730–17736.
45. Derecskei B, Derecskei-Kovacs A. Molecular modeling simulations to predict the density and solubility parameters of ionic liquids. *Mol Simulat*. 2008;34(10–15):1167–1175. Also in: Meunier M, editor. *Industrial Application of Molecular Simulations*. CRC Press, Taylor & Francis Group, 2012. pp 61–76.
46. Bader RFW. Atoms in molecules. *Acc Chem Res*. 1985;18(1):9–15.
47. Bader RFW. A bond path: a universal indicator of bonded interactions. *J Phys Chem A*. 1998;102(37):7314–7323.
48. Green ME. Partially charged $H_5O_2$ as a chemical switch: a bond order and atoms in molecules study of hydrogen bonding determined by surrounding groups. *J Phys Chem A*. 2002;106(46): 11221–11226.
49. Aparicio S, Atilhan M, Khraisheh M, Alcalde R, Fernandez J. Study on hydroxylammonium-based ionic liquids. II. Computational analysis of $CO_2$ absorption. *J Phys Chem B*. 2011;115(43):12487–12498.
50. Arnold WD, Oldfield E. The chemical nature of hydrogen bonding in proteins via NMR: J-couplings, chemical shifts, and AIM theory. *J Am Chem Soc*. 2000;122(51):12835–12841.
51. Klamt A. COSMO-RS: From Quantum chemistry to Fluid Phase Thermodynamics and Drug Design. Amsterdam, The Netherlands: Elsevier Science, 2005.
52. Yu GR, Zhang SJ, Zhou GH, Liu XM, Chen XC. Structure, interaction and property of amino-functionalized imidazolium ILs by molecular dynamics simulation and ab initio calculation. *AIChE J*. 2007;53(12):3210–3221.

53. Tsuzuki S, Tokuda H, Mikami M. Theoretical analysis of the hydrogen bond of imidazolium C2-H with anions. *Phys Chem Chem Phys.* 2007;9(34):4780–4784.
54. Jalili AH, Safavi M, Ghotbi C, Mehdizadeh A, Hosseini-Jenab M, Taghikhani V. Solubility of $CO_2$, $H_2S$, and their mixture in the ionic liquid 1-octyl-3-methylimidazolium bis(trifluoromethyl)sulfonylimide. *J Phys Chem B*. 2012;116(9):2758–2774.
55. Rowland RS, Taylor R. Intermolecular nonbonded contact distances in organic crystal structures: comparison with distances expected from van der Waals radii. *J. Phys. Chem.* 1996;100(18):7384–7391.
56. Stone AJ. Computation of charge-transfer energies by perturbation theory. *Chem Phys Lett.* 1993;211(1):101–109.
57. Zhang X, Huo F, Liu Z, Wang W, Shi W, Maginn EJ. Absorption of $CO_2$ in the ionic liquid 1-n-Hexyl-3-methylimidazolium tris(pentafluoroethyl)tri- fluorophosphate ([hmim][FEP]): a molecular view by computer simulations. *J Phys Chem B*. 2009;113(21):7591–7598.
58. Yuan X, Zhang S, Chen Y, Lu X, Dai W, Mori R. Solubilities of gases in 1,1,3,3-tetramethylguanidium lactate at elevated pressures. *J Chem Eng Data*. 2006;51(2):645–647.
59. Meunier M. Diffusion coefficients of small gas molecules in amorphous cis-1,4-polybutadiene estimated by molecular dynamics simulations. *J Chem Phys.* 2005;123:134906.
60. Zhou ZB, Matsumoto H, Tatsumi K. Cyclic quaternary ammonium ionic liquids with perfluoroalkyltrifluoroborates: synthesis, characterization, and properties. *Chem Eur J*. 2006;12(8):2196–2212.
61. Dzyuba SV, Bartsch RA. Influence of structural variations in 1-alkyl(aralkyl) − 3-methylimidazolium hexafluorophosphates and bis(-trifluoromethylsulfonyl)imides on physical properties of the ionic liquids. *ChemPhysChem.* 2002;3(2):161–166.
62. Kulkarni PS, Branco LC, Crespo JG, Nunes MC, Raymundo A, Afonso CAM. Comparison of physicochemical properties of new ionic liquids based on imidazolium, quaternary ammonium, and guanidinium cations. *Chem Eur J*. 2007;13(30):8478–8488.
63. Matsumoto H, Kageyama H, Miyazaki Y. Room temperature ionic liquids based on small aliphatic ammonium cations and asymmetric amide anions. *Chem Commun.* 2002;(16):1726–1727.
64. Le ML, Alloin F, Strobel P, Lepretre JC, Perez del Valle C, Judeinstein P. Structure-properties relationships of lithium electrolytes based on ionic liquid. *J Phys Chem B*. 2010;114(2):894–903.
65. Yu G, Zhao D, Wen L, Yang S, Chen X. Viscosity of ionic liquids: Database, observation, and quantitative structure-property relationship analysis. *AIChE J*. 2012;58(9):2885–2899.

*Manuscript received Aug. 1, 2012, and revision received Mar. 20, 2013.*